Chinese Chemical Letters 32 (2021) 3833–3836

Contents lists available at ScienceDirect

Chinese Chemical Letters

journal homepage: www.elsevier.com/locate/cclet

Communication

Robust photocatalytic hydrogen production on metal-organic layers of Al-TCPP with ultrahigh turnover numbers

Hui Yu[a,b], Xiang Wu[a,b], Qiaoqiao Mu[a,b], Zhihe Wei[a,b], Yindong Gu[a,b], Xuzhou Yuan[a,b], Yongtao Lu[a,b,*], Zhao Deng[a,b], Yang Peng[a,b,*]

[a] Soochow Institute for Energy and Materials Innovations, College of Energy, Soochow University, Suzhou 215006, China
[b] Key Laboratory of Advanced Carbon Materials and Wearable Energy Technologies of Jiangsu Province, Soochow University, Suzhou 215006, China

ARTICLE INFO

Article history:
Received 27 April 2021
Revised 11 May 2021
Accepted 18 May 2021
Available online 25 May 2021

Keywords:
Photocatalysis
Metal organic layers
Al-TCPP
Hydrogen production
Turnover numbers

ABSTRACT

The development of robust photocatalytic systems is key to harvest the solar power for hydrogen production. In the current study, a series of aluminum-based porphyrinic metal organic frameworks (Al-TCPP) with various morphologies of bulk, carambola-like and nanosheets are synthesized with modulated layer thickness. Morphology-dependent photocatalytic activities in hydrogen production are witnessed and inversely correlate to the thickness of the Al-TCPP micro-platelets or nanosheets. Particularly, the exfoliated metal organic layers (MOLs) of Al-TCPP demonstrated a high hydrogen yield rate of 1.32×10^4 μmol h^{-1} g^{-1} that is 21-fold of that from the bulk catalyst, as well as an exceptional TON of 6704 that seldom seen in literature. Through comprehensive photochemical characterizations, the remarkable photocatalytic performance of Al-TCPP-MOL is attributed to the great charge separation efficiency and transfer kinetics endowed by the ultrathin 2D morphology with extended active surface area.

Photocatalytic hydrogen production by directly utilizing the solar energy has been long pursued as the most ideal manner to address the exorbitant exploitation of fossil-based energy sources that besets the mankind [1]. However, as of today, the progress has been still severely impeded by the lack of efficient photocatalysts with high quantum yield [2]. A practical photocatalyst should possess the optimal attributes in all the three key steps of photocatalysis, namely, light harvesting, photocarrier separation and transportation, as well as redox charge transfer [3,4]. Great efforts have been devoted to coordinate and synchronize these processes by devising photocatalysts of various architectures and compositions [5–7], but more practical solar efficiency, catalyst stability, as well as mechanistic understanding are needed to techno-economically harness the technology [8].

Among the enormous photocatalysts that have been explored [9–16], semi-conducting metal-organic frameworks (MOFs) represent a unique opportunity due to their high porosity and surface area, isolated and often under-coordinated metal nodes, well-defined topological structure, as well as tunable chemical functionalities, offering a versatile knob to regulate and steer the photocatalytic processes [17–19]. In particular, MOFs constructed with porphyrin-containing ligands often possess strong light-absorbing properties, and are generally photoactive in mimicking the natural photosynthetic process [20]. For this reason, many investigations have been carried out using porphyrin-based MOFs as the photocatalysts for hydrogen production [21–27] and CO_2 reduction [28,29]. Despite the great advances demonstrated by these studies, MOFs, especially in the bulk form, contain intrinsic limitations in low charge mobility, poor stability and concealed active sites [18,19]. Alternately, 2D metal-organic layers (MOLs) might stand for a better option for this purpose owing to the drastically improved charge separation efficiency and highly exposed active sites [30–32], provided that the stability issue can be also properly addressed. Nevertheless, MOLs based on porphyrin derivatives have been barely reported.

In the current work, MOFs of Al-TCPP (TCPP = tetrakis(4-carboxylphenyl) porphyrin) with different morphologies, spanning across bulk micro-platelets, clustered nanosheets and ultrathin MOLs, are synthesized by chemical and physical methods with modulated layer thickness. Their capabilities in catalyzing hydrogen production under visible light are carefully scrutinized, revealing morphology-dependent photocatalytic activities. Remarkably, Al-TCPP in the MOL form demonstrates the best photocatalytic performance, achieving an outstanding hydrogen yield rate of 1.32×10^4 μmol h^{-1} g^{-1} and a superb long term stability with an exceptional TON of 6704. Various spectroscopic and electrochem-

* Corresponding authors.
E-mail addresses: sudalyt@suda.edu.cn (Y. Lu), ypeng@suda.edu.cn (Y. Peng).

https://doi.org/10.1016/j.cclet.2021.05.035
1001-8417/

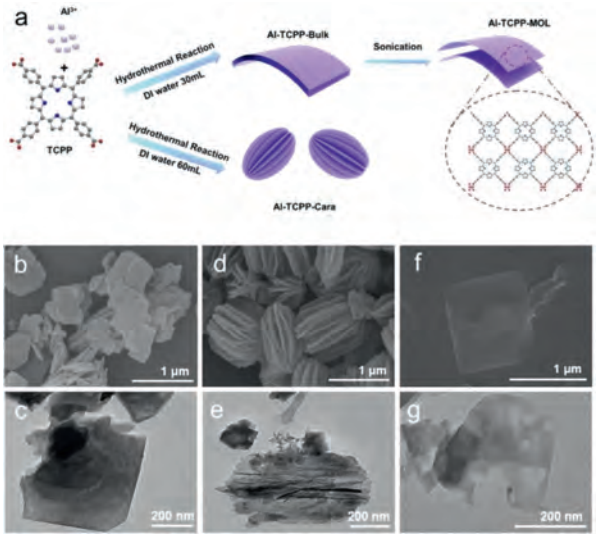

Fig. 1. Preparation of the Al-TCPP photocatalysts with various morphologies. (a) Schematic illustration of the synthetic procedures. SEM images of (b) Al-TCPP-Bulk, (d) Al-TCPP-Cara and (f) Al-TCPP-MOL; TEM images of (c) Al-TCPP-Bulk, (e) Al-TCPP-Cara and (g) Al-TCPP-MOL.

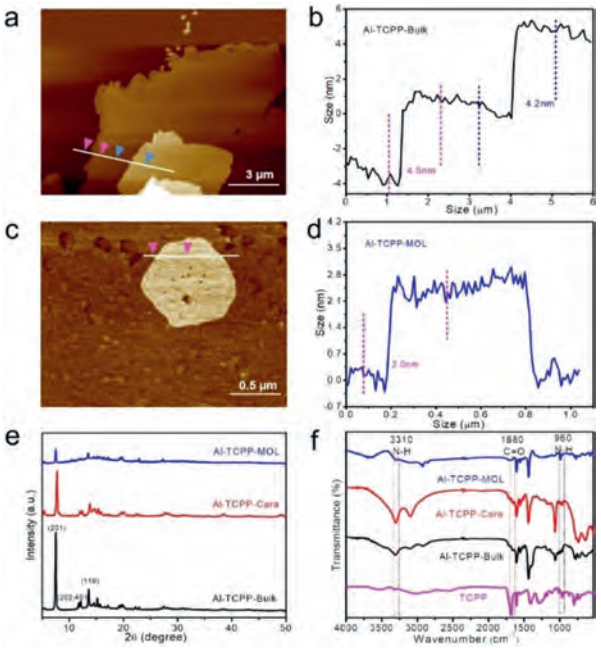

Fig. 2. Structural characterizations of the photocatalysts. AFM topographic image and the corresponding height profile of (a, b) Al-TCPP-Bulk and (c, d) Al-TCPP-MOL, respectively. (e) XRD patterns of Al-TCPP-Bulk, Al-TCPP-Cara and Al-TCPP-MOL. (f) FT-IR spectra of TCPP, Al-TCPP-Bulk, Al-TCPP-Cara and Al-TCPP-MOL.

ical techniques are further exploited to elucidate the greatly enhanced photocatalytic activity on the Al-TCPP MOLs.

Al-TCPP-Bulk was synthesized by the hydrothermal method illustrated in Fig. 1a and detailed in the experimental section (Supporting information). The as-obtained product displayed a platelet morphology comprising stacked 2D nanosheets, which are visualized from the SEM (Fig. 1b), TEM (Fig. 1c) and AFM (Fig. 2a) images. From the AFM height profile (Fig. 2b), the thickness of each stacked lamellar sheet in Al-TCPP-Bulk is 4.2 ± 0.3 nm. Interestingly, by simply changing the volume of the water solvent employed in the hydrothermal reaction, the product can change to a carambola-like morphology with numerous nanosheets of

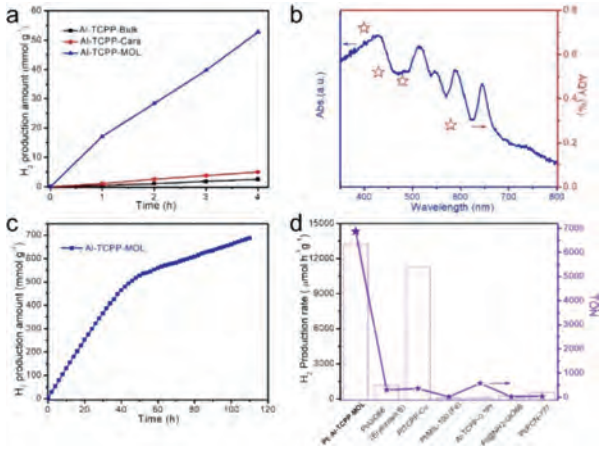

Fig. 3. Performances of photocatalytic H_2 production. (a) H_2 yield of Al-TCPP-Bulk, Al-TCPP-Cara and Al-TCPP-MOL in 4 h normalized to the catalyst weight. (b) Wavelength-dependent AQY of Al-TCPP-MOL at 420, 450, 500 and 600 nm. (c) Prolonged photocatalytic H_2 production over Al-TCPP-MOL (5 mg). The hole scavenger of ascorbic acid was replenished every 10 h; (d) Comparison of the photocatalytic H_2 production rate and TON among Al-TCPP-MOL and other MOF-based photocatalysts reported in literature.

12.5 ± 5 nm vertically converged together (Figs. 1d and e), and is thus denoted as Al-TCPP-Cara. Furthermore, Al-TCPP-Bulk can be exfoliated into thin nanosheets through ultrasonication, displaying semi-transparent irregular shapes in both SEM (Fig. 1f) and TEM (Fig. 1g) images. AFM measurements revealed a few defective pinholes on the exfoliated nanosheets with an average thickness of 2.2 ± 0.2 nm indicative of monolayer structure (Figs. 2c and d, Fig. S2 in Supporting information), denoted as Al-TCPP-MOL (MOL: metal-organic layers).

X-ray diffraction (XRD) revealed similar diffraction patterns of Al-TCPP-Bulk, Al-TCPP-Cara, and Al-TCPP-MOL (Fig. 2e), of which the peaks at $2\theta = 7.43°$ and 13.67° are respectively corresponding to the (201) and (110) planes of Al-TCPP reported in the literature [33,34]. Note that the intensity of the Al-TCPP-MOL peaks with slightly down-shifted 2θ angles is much lower than those of Al-TCPP-Bulk and Al-TCPP-Cara, coinciding with the exfoliated state of the MOF as witnessed previously by microscopies. Fourier transform infrared spectra (FT-IR) in Fig. 2f show the carbonyl (C=O) stretching of -COOH at 1680 cm^{-1} is severely damped in all forms of Al-TCPP when compared to that of the TCPP ligand, indicating in the MOFs the carboxylate groups of TCPP are mostly coordinated with Al^{3+}. The peaks at 3310 and 960 cm^{-1}, respectively corresponding to the stretching and in-plane vibration modes of –NH in the freebase porphyrin rings [33], are distinguishable from all samples and indicate Al^{3+} does not coordinate with the pyrrolic N in the porphyrin ring. Taken together from the above microscopic and spectroscopic studies, we can conclude that Al-TCPP-Bulk, Al-TCPP-Cara and Al-TCPP-MOL differ only in morphology, but not in composition.

Performances of photocatalytic hydrogen production were assessed for Al-TCPP-Bulk, Al-TCPP-Cara and Al-TCPP-MOL using photo-deposited Pt nanoparticles (2 wt%) as the co-catalyst and ascorbic acid as the hole scavenger. In the four-hour photocatalytic tests with a band-pass filter of 420 nm, Al-TCPP-MOL, among all the three photocatalysts, demonstrated the best hydrogen yield rate of 1.32×10^4 μmol h^{-1} g^{-1} (Fig. 3a), which is 21-fold of that for Al-TCPP-Bulk (650 μmol h^{-1} g^{-1}) and 11-fold of that for Al-TCPP-Cara (1250 μmol h^{-1} g^{-1}). Al-TCPP-MOL is also ranked amongst the top of MOF-based photocatalysts reported today for hydrogen production (Fig. 3d, Table S1 in Supporting information). It is thus evident the photocatalytic activity of Al-TCPP is

morphology-dependent, and inversely correlates to the thickness of the MOF platelets or sheets. To further explore the role of each component in our photocatalytic system, a series of control experiments were conducted by varying the experimental parameters (Fig. S3 in Supporting information). First, in the absence of Pt as the co-catalyst, the hydrogen production rate of Al-TCPP-MOL was only 0.008 mmol h^{-1} g^{-1}, whereas that of the complete photocatalytic system was 13.2 mmol h^{-1} g^{-1}, signifying the important role of the co-catalyst. Second, when either the photocatalyst or sacrificial agent was absent, no gaseous products were obtained. Third, in absence of the hole sacrificial agent, Pt/Al-TCPP-MOL failed to produce hydrogen under light conditions. This result proves that the presence of ascorbic acid is necessary to consume photo-generated holes and plays a vital role in the production of hydrogen. Finally, our experimental results show that when only TCPP was employed as the photosensitizer, only 0.064 mmol h^{-1} g^{-1} hydrogen was produced. This result indicates the formation of MOF structure significantly promotes light harvesting and photoelectron utilization.

Fig. 3b shows the wavelength-dependent apparent quantum yield (AQY) measured for Al-TCPP-MOL at 420, 450, 500 and 600 nm, being 0.72%, 0.52%, 0.48% and 0.28%, respectively (Table S2 in Supporting information). Note that the observed wavelength-dependence of AQY well coincides with the UV–vis diffuse reflectance spectrum (DRS) of Al-TCPP-MOL, justifying the photo-driven HER processes. More remarkably, Al-TCPP-MOL manifested a remarkable photocatalytic stability, capable of producing hydrogen continuously given the adequately added hole scavenger. As shown in Fig. 3c, Al-TCPP-MOL was able to function continuously for a total period of 110 h with intermittently replenished ascorbic acid, accounting for a TON of at least 6704 (based on the amount of Pt quantified by ICP), which is among the best reported in literature (Fig. 3d). After the prolonged photocatalytic reaction, both XRD and FTIR show the structure of Al-TCPP-MOL was well preserved (Fig. S4 in Supporting information), endorsing its superb structural durability, apart from the remarkable catalytic stability, in the aqueous photocatalytic system applied here. We also note that the ascorbic acid chosen here as the hole scavenger is very crucial for the witnessed high catalytic activity and stability. Swapping it to triethanolamine (TEOA) would drastically curtail the overall catalytic performance, signifying the importance of a properly configured photocatalytic system.

To further interrogate the enhanced performance seen on Al-TCPP-MOL, the optical absorption, band structure, and photoexcited charge separation and transfer were compared for all photocatalysts by using UV–vis spectroscopy, Mott-Schottky plots, photoluminescence spectrometry (PL), transient photocurrent response (TPR) and electrochemical impedance spectra (EIS). First of all, UV–vis DRS spectra showed all Al-TCPP samples contain Soret peak at 420 nm ($S_0 \rightarrow S_2$ absorption) and other bands in the longer wavelengths (420–800 nm) ascribed to the Q bands ($S_0 \rightarrow S_1$ absorption), which are the characteristic of porphyrin units (Fig. 4a) [33]. By converting the DRS spectra into Tauc plots, the band gap of the photocatalysts can be derived, giving E_g values of 1.46, 1.42 and 1.47 eV for Al-TCPP-Bulk, Al-TCPP-Cara, and Al-TCPP-MOL, respectively (Fig. S5 and Table S3 in Supporting information). Second, Mott-Schottky (M-S) plots were acquired to estimate the flat band potentials (E_{fb}) of the photocatalysts, which are typically positioned 0.1–0.2 V below the conductive band minimum (CBM) for the n-type semiconductor. All samples of Al-TCPP-Bulk, Al-TCPP-Cara, and Al-TCPP-MOL display positive slopes in the M-S plots (Figs. S6a-c in Supporting information), affirming their n-type semi-conductive nature. Accordingly, the E_{fb} were measured at −0.76, −0.76 and −0.78 V (*vs.* NHE, pH 7.0) for the above three samples, respectively. Lastly, combining the values of E_g and E_{fb}, the CBM and VBM (valence band maximum) can be deduced for all photocatalysts, with their band structure illustrated in Fig. S6d

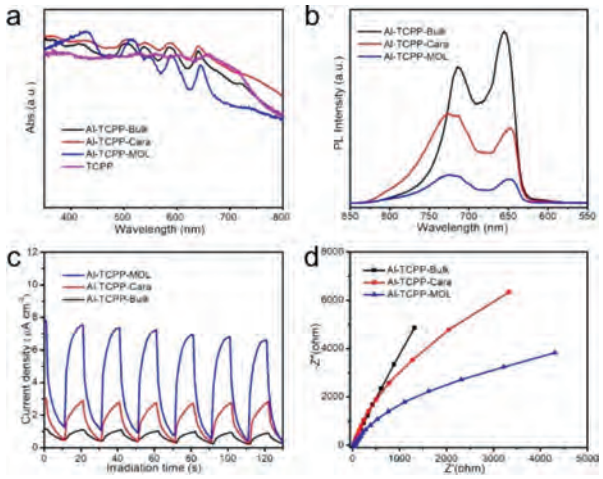

Fig. 4. Mechanistic investigation of the photocatalytic processes. (a) UV–vis diffuses reflectance spectra of all the Al-TCPP and TCPP samples. (b) Steady-state PL emission spectra, (c) Transient photocurrent responses, and (d) EIS Nyquist plots of Al-TCPP-Bulk, Al-TCPP-Cara and Al-TCPP-MOL.

(Supporting information) and tabulated in Table S3. Note that all the CBM values of Al-TCPP-Bulk, Al-TCPP-Cara, and Al-TCPP-MOL are lower than the equilibrium potential of H^+/H_2 (−0.41 V *vs.* NHE, pH 7.0), attesting to their capabilities in driving H_2 formation. Owing to the similar band structure and UV–vis absorption of all three photocatalysts, we consider light absorption is not the major cause of the observed difference in photocatalytic behaviors.

Next, we seek to investigate the efficiencies of photoexcited charge separation and transfer for all the three photocatalysts. Fig. 4b shows the steady-state PL spectra taken at an excitation wavelength of 420 nm, showing the order of emission intensity follows Al-TCPP-Bulk > Al-TCPP-Cara > Al-TCPP-MOL. This suggests the radiant combination of photo-generated carriers in Al-TCPP-MOL is less populated than that in Al-TCPP-Cara and Al-TCPP-MOL, or in other words, more photo-generated carriers in Al-TCPP-MOL are quenched by structural defects and dangling bonds, which coincides with its highest ECSA that will be detailed later. TPR measurements shown in Fig. 4c further corroborate the remarkably enhanced charge separation efficiency in Al-TCPP-MOL, displaying the highest photocurrent response larger than 7.0 μA/cm^2 during the whole six light-on-off cycles, which is more than two folds higher than that observed for Al-TCPP-Cara (2.8 μA/cm^2), and 6-fold of that on Al-TCPP-Bulk (1.2 μA/cm^2).

Finally, electrochemical impedance spectroscopy (EIS) were carried out to probe the charge transfer kinetics in the photocatalysts upon illumination. Comparing to Al-TCPP-Bulk and Al-TCPP-Cara, Al-TCPP-MOL displays the lowest slope, reflecting the smallest charge transfer impedance [35]. In addition, electrochemical specific surface area of the photocatalysts estimated by taking cyclic voltammetry (CV) at different scan rates in the non-Faradaic regime shows the electrochemical double-layer capacitance of Al-TCPP-MOL (4.12 mF/cm^2) is nearly doubled and quadrupled when compared to those of Al-TCPP-Cara (2.14 mF/cm^2) and Al-TCPP-Bulk (1.28 mF/cm^2), respectively, further attesting to the improved charge transfer kinetics (Fig. S7 in Supporting information). Thus, collectively from the results of PL, TPR, EIS and ECSA, we can come up with the conclusion that the charge separation efficiency in Al-TCPP-MOL is the highest among the three photocatalysts, in virtue of its ultrathin 2D morphology, and contribute majorly to the observed performance enhancement in photocatalytic hydrogen production.

In summary, Al-TCPP of various morphologies were synthesized and employed as the catalysts for photocatalytic hydro-

gen production. Morphology-dependent photocatalytic activity was witnessed, and inversely correlates to the thickness of the MOF micro-platelets or nano-sheets. Particularly, the exfoliated Al-TCPP-MOL with monolayer thickness demonstrated remarkable hydrogen yield rate of 1.32×10^4 μmol h^{-1} g^{-1}, which is 21-fold of that for Al-TCPP-Bulk and 11-fold of that for Al-TCPP-Cara, and ranked among the best seen for MOF-based photocatalysts. More impressively, superb catalytic stability and structural durability were realized for Al-TCPP-MOL, delivering an exceptional TON of 6704 that is seldom seen in literature. Lastly, the greatly enhanced photocatalytic performance on Al-TCPP-MOL was elucidated via comprehensive characterizations on optical absorption, band structure, and charge mobility, attributing to the great charge separation efficiency and transfer kinetics endowed by the ultrathin 2D morphology with extended active surface area.

Declaration of competing interest

The authors have no conflicts of interest to declare.

Acknowledgments

This work was financially supported by National Natural Science Foundation of China (Nos. 22072101, 22075193, 51911540473), Natural Science Research Project of Jiangsu Higher Education Institutions of China (No. 18KJA480004), the Key Technology Initiative of Suzhou Municipal Science and Technology Bureau (No. SYG201934) Six Talent Peaks Project in Jiangsu Province (No. TD-XCL-006) and Priority Academic Program Development (PAPD) of Jiangsu Higher Education Institutions.

Supplementary materials

Supplementary material associated with this article can be found, in the online version, at doi:10.1016/j.cclet.2021.05.035.

References

[1] C. Acar, I. Dincer, G.F. Naterer, Int. J. Energ. Res. 40 (2016) 1449–1473.
[2] Y. Zheng, P.Z. Wang, Chin. J. Catal. 34 (2013) 524–535.
[3] X. Chen, S. Shen, L. Guo, S.S. Mao, Chem. Rev. 110 (2010) 6503–6570.
[4] A.A. Ismail, D.W. Bahnemann, Sol. Energ. Mat. Sol. C 128 (2014) 85–101.
[5] Z. Wang, C. Li, K. Domen, Chem. Soc. Rev. 48 (2019) 2109–2125.
[6] Q. Wang, K. Domen, Chem. Rev. 120 (2020) 919–985.
[7] A. Kubacka, M. Fernández-García, G. Colón, Chem. Rev. 112 (2012) 1555–1614.
[8] L.J. Guo, Y.B. Chen, J.Z Su, M.C. Liu, Y. Liu, Energy 172 (2019) 1079–1086.
[9] A. Naldoni, M. Altomare, G. Zoppellaro, et al., ACS Catal. 9 (2019) 345–364.
[10] J.A. Nasir, Z.U. Rehman, S.N.A. Shah, et al., J. Mater. Chem. A 8 (2020) 20752–20780.
[11] S. Wang, J. Zhang, B. Li, H. Sun, S. Wang, Energy Fuel 35 (2021) 6504–6526.
[12] Q. Xiang, J. Yu, J. Phys. Chem. Lett. 4 (2013) 753–759.
[13] T. He, K. Geng, D. Jiang, ACS Mater. Lett. 1 (2019) 203–208.
[14] P. Ganguly, M. Harb, Z. Cao, et al., ACS Energy Lett. 4 (2019) 1687–1709.
[15] X. Wang, C. Zhou, R. Shi, et al., Nano Res. 12 (2019) 2385–2389.
[16] X.S. Wang, C. Zhou, R. Shi, Q.Q. Liu, T.R. Zhang, Rare Metal. 38 (2019) 397–403.
[17] Q. Mu, Y. Su, ;.Z. Wei, et al., J. Catal. 397 (2021) 128–136.
[18] W. Zhu, C. Zhang, Q. Li, et al., Appl. Catal. B: Environ. 238 (2018) 339–345.
[19] Y. Ma, Y. Lu, G. Hai, et al., Sci. Bull. 65 (2020) 658–669.
[20] L. Wang, H. Fan, F. Bai, MRS Bull. 45 (2020) 49–56.
[21] Q. Zuo, T. Liu, C. Chen, et al., Angew. Chem. Int. Ed. 58 (2019) 10198–10203.
[22] P. Liao, Y. Hu, Z. Liang, et al., J. Mater. Chem. A 6 (2018) 3195–3201.
[23] T. He, S. Chen, B. Ni, et al., Angew. Chem. Int. Ed. 57 (2018) 3493–3498.
[24] X. Fang, Q. Shang, Y. Wang, et al., Adv. Mater. 30 (2018) 1705112.
[25] J.D. Xiao, Q. Shang, Y. Xiong, et al., Angew. Chem. Int. Ed. 55 (2016) 9389–9393.
[26] M. Zhu, Y. Du, P. Yang, X. Wang, Catal. Sci. Technol. 3 (2013) 2295–2302.
[27] A. Fateeva, P.A. Chater, C.P. Ireland, et al., Angew. Chem. Int. Ed. 51 (2012) 7440–7444.
[28] X. Zhang, M. Cibian, A. Call, K. Yamauchi, K.P. Sakai, ACS Catal. 9 (2019) 11263–11273.
[29] Y. Kuramochi, Y. Fujisawa, A. Satake, J. Am. Chem. Soc. 142 (2020) 705–709.
[30] X. Wang, X. Zhang, W. Zhou, et al., Nano Energy 62 (2019) 250–258.
[31] H. Hu, Z. Wang, L. Cao, et al., Nat. Chem. 13 (2021) 358–366.
[32] Y. Liu, L. Liu, X. Chen, et al., Y., J. Am. Chem. Soc. 143 (2021) 3509–3518.
[33] N. Sadeghi, S. Sharifnia, T.O. Do, J. Mater. Chem. A 6 (2018) 18031–18035.
[34] Y. Liu, Y. Yang, Q. Sun, et al., ACS Appl. Mater. Interfaces 5 (2013) 7654–7658.
[35] D. Sun, J.W. Shi, D. Ma, et al., Chin. J. Catal. 41 (2020) 1421–1429.